Pramana – J. Phys. (2019) 93:58
https://doi.org/10.1007/s12043-019-1817-0

Studies on the design and parametric effects of a diode pump alkali (rubidium) laser

R BISWAL[1,*], G K MISHRA[1], S K AGRAWAL[2], S K DIXIT[3] and S V NAKHE[4]

[1]Laser Development and Industrial Application Division, Raja Ramanna Centre for Advanced Technology, Indore 452 013, India
[2]Laser Control and Instrumentation Division, Raja Ramanna Centre for Advanced Technology, Indore 452 013, India
[3]Fibre Sensor and Optical Spectroscopy Section, Raja Ramanna Centre for Advanced Technology, Indore 452 013, India
[4]Laser Group, Raja Ramanna Centre for Advanced Technology, Indore 452 013, India
*Corresponding author. E-mail: rbiswal@rrcat.gov.in

MS received 7 July 2018; revised 29 December 2018; accepted 5 April 2019; published online 16 July 2019

Abstract. This paper presents a comprehensive study of the design and parametric investigation of a diode pump alkali laser (DPAL): an emerging, high quantum efficiency, challenging laser system in the near-infrared region with potential for numerous applications. It covers the design and development of a diode pumped alkali (rubidium) laser (Rb:DPAL) gain cell and associated subsystems including the glove box-based alkali transfer set-up. Laser generation (λ∼795 nm) in a continuous wave (CW) mode with end-pumped geometry in the Rb cell is reported. Comparative studies on the Rb-DPAL output were carried out with various critical operating parameters such as buffer gas pressure, buffer gas composition, gain medium temperature and pump power/intensity. The experimental results were analysed and discussed in light of the efficacy of the pump beam absorption, the laser level kinetics and effective lasing volume in the Rb-DPAL gain cell.

Keywords. Diode pump alkali laser; alkali laser; gas laser; optical pumping.

PACS Nos 42.55.Lt; 42.55.−f; 42.60.Jf

1. Introduction

Diode pump alkali (K/Rb/Cs) lasers (DPALs) are high quantum efficiency (∼99.5%/98.1%/95.2%) systems in the near-infrared region (λ∼770/795/895 nm) and have been emerging as highly efficient brightness converters of semiconductor diode lasers [1–5]. These are an entirely new class of challenging lasers based on the excitation of atomic alkali vapours that combine features of both the gas (high beam quality) and the solid-state (diode/optical pumping) lasers [5–7]. Due to higher quantum efficiency, lower operational wavelength, large optical cross-section, lack of stress birefringence and stress fracture, lower refractive index fluctuation and lower size-weight-and-power (SWAP) performance, these lasers are being envisaged as superior substitutes of solid-state and chemical lasers for high power (∼kW–MW class), high beam quality radiations essential for numerous scientific, industrial, defense and aerospace applications [5–10]. DPALs can be used as areal incinerators, for charging remote photovoltaic cells and remote material processing, because of the excellent atmospheric propagation of radiations along with high power, high beam quality and high efficiency capabilities whereas their frequency doubled blue–violet radiations are best suited for underwater material processing and communications. Moderate to low power, narrow linewidth DPALs are best suited for researches in quantum optics, atomic physics and laser spectroscopy, e.g. the production of spin-polarised noble atoms through laser atom cooling, etc., whereas their frequency-doubled blue–violet output find use in medical treatment, environmental monitoring, data recording, etc. [5–13].

In a DPAL, the buffered alkali atoms are optically pumped in their D_2 line, i.e. to their upper level of the first excited state ($np\,^2P_{3/2}$), by a suitable narrow linewidth diode laser, which subsequently undergoes fast collisional relaxation to the lower level of the first excited state ($np\,^2P_{1/2}$). Under suitable conditions,

the lasing action is established in their D_1 line, i.e. between the $np\,^2P_{1/2}$ and the ground state ($ns\,^2S_{1/2}$) [2–7]. Since their conceptualisation/first-demonstration in 2001/2005 (Rb-DPAL) [1,2], followed by concomitant development in high power diode laser technology, to date, DPALs of average power as high as ∼30 kW (Rb-DPAL) [11] and ∼1.5–2 kW from K- and Cs-DPAL with slope efficiencies of ∼50% [9] have been demonstrated whereas a design for Rb-DPAL of 2 MW average power has been proposed [12]. For realising such systems, several challenging issues are involved. Apart from the required pump diode system, the most crucial are efficient design of the laser gain medium, efficient handling/transferring of highly reactive alkali metal (lasant) into the gain cell followed by the identification of appropriate operating conditions for the efficient absorption of the pump beam. These are followed by mitigating challenges of establishing laser gain by tailoring the laser kinetics (collision relaxation and mixing of the upper levels, $np\,^2P_{3/2}$ and $np\,^2P_{1/2}$) through varied buffer gas compositions (due to narrow Doppler-broadened gain bandwidth of ∼10 GHz for alkalis and quasi-two-level nature of DPALs). In the literature, various aspects of DPALs ranging from the pumping configurations, power scaling and beam characterisation to simulation studies are available. However, comprehensive studies on the laser system design and exclusive parametric effects are missing [1–13].

With these perspectives and challenges in view, development studies of one of the DPALs, i.e. Rb-DPAL, was taken up based on the judicious choice of a commercially available pump diode laser. In this paper, comprehensive studies of such a complex system encompassing the design and development of the Rb-DPAL gain cell, alkali handling set-up and other associated control systems, followed by investigations of the effects of various operating parameters on laser output were carried out in continuous wave (CW) mode with end-pumped geometry. The experimental results were analysed and discussed by taking into account the efficacy of the pump beam absorption, related laser level kinetics and effective laser gain volume.

2. Physics of Rb-DPAL

The schematic of the energy levels showing the pump and lasing transitions in Rb-DPAL is shown in figure 1. The first excited levels ($5p\,^2P_{3/2}$ and $5p\,^2P_{1/2}$) have energies of 12816.56 and 12578.96 cm^{-1} with a small separation of about 237.6 cm^{-1} [2–4]. Both levels are strongly electric-dipole coupled to the ground state ($5s\,^2S_{1/2}$). In Rb-DPAL, the rubidium atoms are

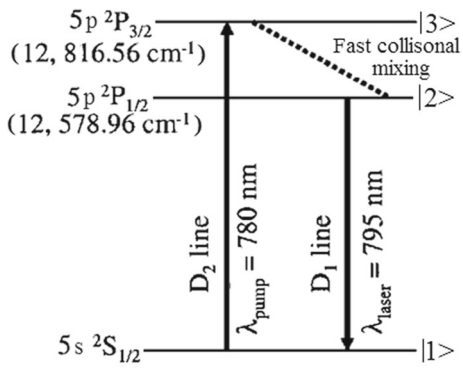

Figure 1. Schematic energy level diagram of Rb-DPAL.

resonantly excited in their D_2 line ($5s\,^2S_{1/2} \rightarrow 5p\,^2P_{3/2}$) by using an appropriate pump diode laser (AlGaAs, $\lambda \sim 780$ nm). The excited rubidium atoms subsequently undergo fast mixing with level $5p\,^2P_{1/2}$ through collision with buffer gas species (He and/or C_2H_6/CH_4) and establish population inversion in their D_1 line ($5p\,^2P_{1/2} \rightarrow 5s\,^2S_{1/2}$). Under the lasing condition, the collisional mixing rate was faster than the spontaneous decay rate ($\sim 3.8 \times 10^7\ s^{-1}$) and the stimulated emission rate ($\sim 1.8 \times 10^8\ s^{-1}$) [5,6,14,15]. In addition, the buffer gases also broaden the atomic transitions (D_2) enhancing the absorption of the pump diode beam.

3. Development of subsystems for Rb-DPAL

The Rb-DPAL system mainly consists of a laser gain cell, separate precision heating arrangements for the gain cell and its windows, an efficient rubidium handling system, a gas handling set-up and a precision electronic arrangement to control the associated parameters, in addition to the pump diode laser and necessary optics. Figures 2A and 2B show the schematic drawing of the typical Rb-DPAL gain cell and photograph of the cell–heater–window assembly, respectively. The SS-316 gain cell had an inner/outer diameter of 25/50 mm and a length of 25 mm with tapered end faces (about 5° with respect to vertical) for mounting of the end windows. It had a side arm reservoir (10 mm internal diameter, 25 mm length) for rubidium at the bottom and several through holes (4.6 mm diameter) for the insertion of specially designed fused-silica encapsulated, nichrome wire based microheater cartridges (4.5 mm diameter and 20–25 mm length: inset of figure 2Ba). Fused silica end windows (10 mm thickness, 35 mm diameter), with heating elements embedded along their circumferences (inset of figure 2Bb), sealed the alkali cell by O-rings. There was provision for gas inlet/outlet through an isolation valve.

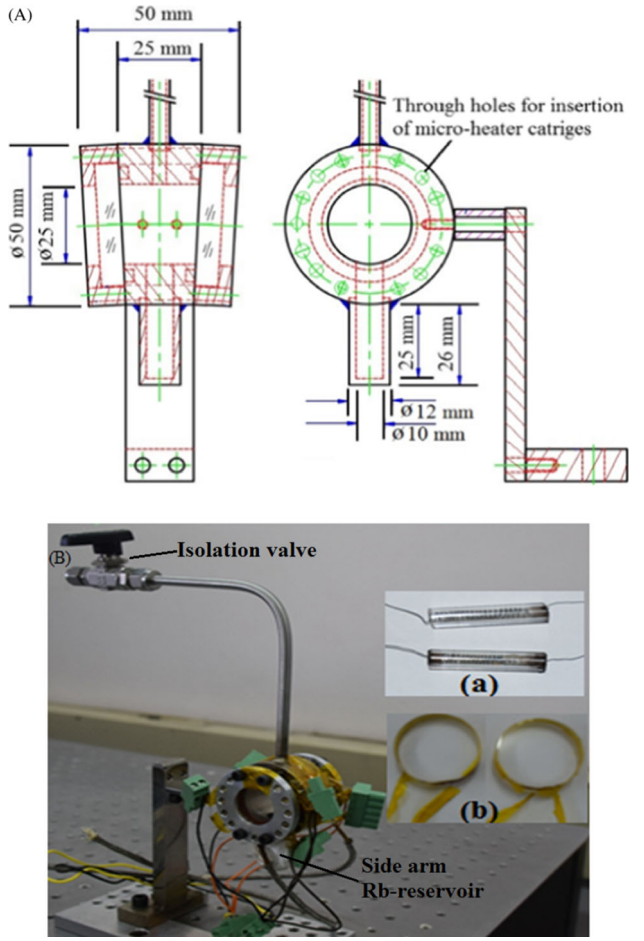

Figure 2. Rb-DPAL gain cell: (**A**) Schematic drawing and (**B**) photograph of the assembly (inset: (**a**) microheaters and (**b**) laser windows with heater element).

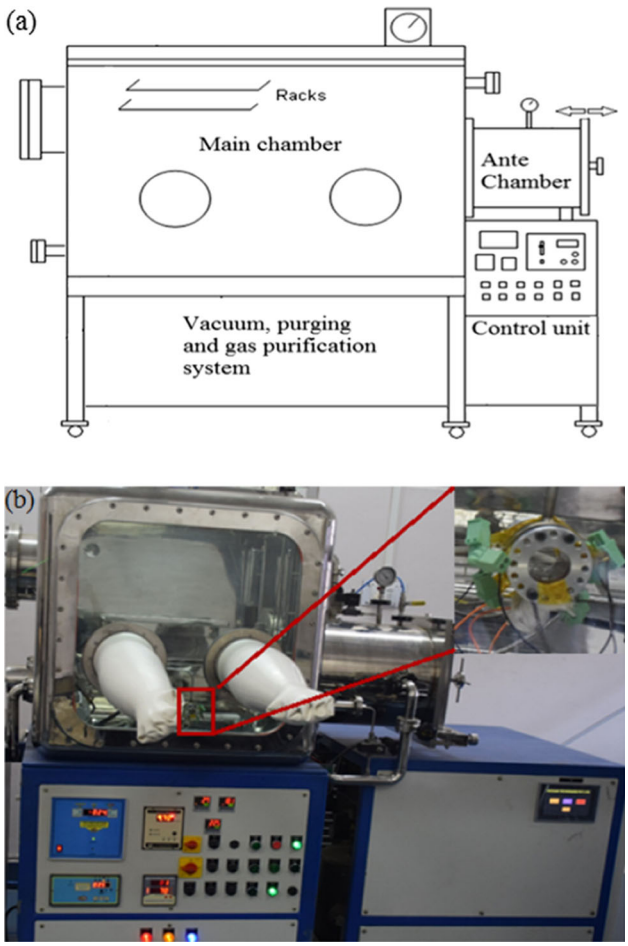

Figure 3. (**a**) Schematic and (**b**) photograph of the glove box system for the transfer of rubidium (inset: DPAL cell with filled rubidium inside the glove box).

The cell assembly was thoroughly cleaned ultrasonically, baked, evacuated and tested for a leak rate of $\sim 10^{-9}$ mbar l/s and pressure withstanding integrity of ~4 bar of He by using a mass spectrometer leak detector. This was followed by transferring high-purity (99.75%) rubidium (M/s Alfa Aesar, USA) in a special set-up consisting of a glove box (figures 3a and 3b) with control of the residual moisture and oxygen level down to ~20 ppm. A procedure was developed to maintain the purity of the loaded rubidium in the gain cell.

4. Experimental arrangement

The schematic of the experimental set-up for the Rb-DPAL is shown in figure 4. A commercially available CW diode laser ($\lambda \sim 780 \pm 0.3$ nm) (M/s DILAS), whose linewidth was narrowed ($\Delta\lambda \sim 0.6$ nm full width at half maximum (FWHM)) by using a volume Bragg grating (VBG), was used as the pump source (4 in figure 4). The diode laser beam was coupled through an optical fibre (core diameter (D_{core}) = 600 μm, numerical aperture (NA) = 0.22) and the output was collimated using a spherical lens (L1) of focal length (f_1) = 10 cm. The laser active medium was end-pumped by using a pair of beam splitting cube polarisers (P1 and P2) and spherical lens (L2). Although both end pumping and transverse pumping are used in DPALs, the choice of the former is a trade-off between better pump absorption, efficiency and beam quality vs. higher input/output power albeit with inferior beam quality and efficiency [7]. The optical resonator consisted of a high reflecting plane mirror (HR, reflectivity >99%) and a plane output coupler (OC) of reflectivity ~60%, separated by a distance of about 30 cm. The intracavity cube polariser P2 reflected the 780 nm s-polarised pump beam into the laser gain cell and allowed the transmission of a 795-nm Rb-DPAL beam to build up with orthogonal (p) polarisation. The laser emission as well as its beam intensity were monitored using a fibre-coupled

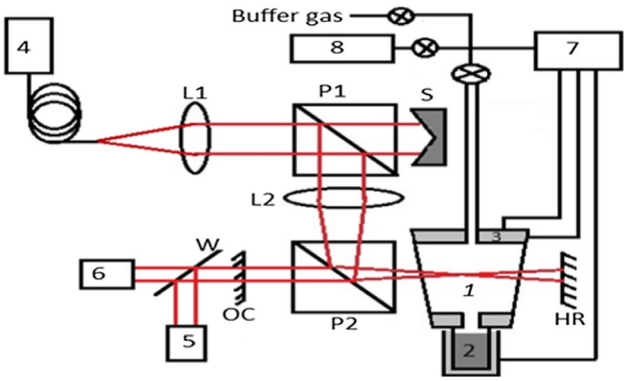

Figure 4. Schematic of the experimental set-up of the developed Rb-DPAL system.

spectrophotometer (Avantes: Avaspec 3648) and a CCD camera (5), with suitable attenuation using neutral density filters, and an infrared sensor (Newport: F-IRC4) (6), both placed at a distance of about 30 cm from the OC.

The experiments were carried out by changing buffer gas pressure and its composition, rubidium reservoir temperature and pump power/intensity. The buffer gas pressure was varied from 0.3 to 4 bar for pure He, pure C_2H_6 and a mixture of He and C_2H_6 with varying compositions (10–25% C_2H_6 + He (balance)). The temperature of the rubidium reservoir was varied from 70 to 150°C and the pump power was varied within 6–8 W (s-polarised power into the laser cell), which was coupled to the laser gain cell using two different convex lenses of focal length (f_2) values of 10 and 15 cm (L2) for different buffer gases. In all the cases, the temperatures of the cell body and windows were maintained at ∼5°C higher than that of the rubidium reservoir.

5. Experimental results and discussion

5.1 *Laser generation*

The photograph of the developed Rb-DPAL system with highly directional output beam, as seen on the infrared sensor (inset: right bottom) is shown in figure 5a. The recorded optical spectrum and the CCD image of the laser output beam cross-section intensity are shown in figure 5b. Following the absorption of the pump diode beam, fluorescence peaks at ∼780 and ∼795 nm were observed for various parametric conditions. However, the lasing action was realised beyond certain threshold values of the pump power/intensities. This was adjudged by the alignment/misalignment of the optical resonator/output coupler, i.e. with/without the optical feedback. Depending on the operating

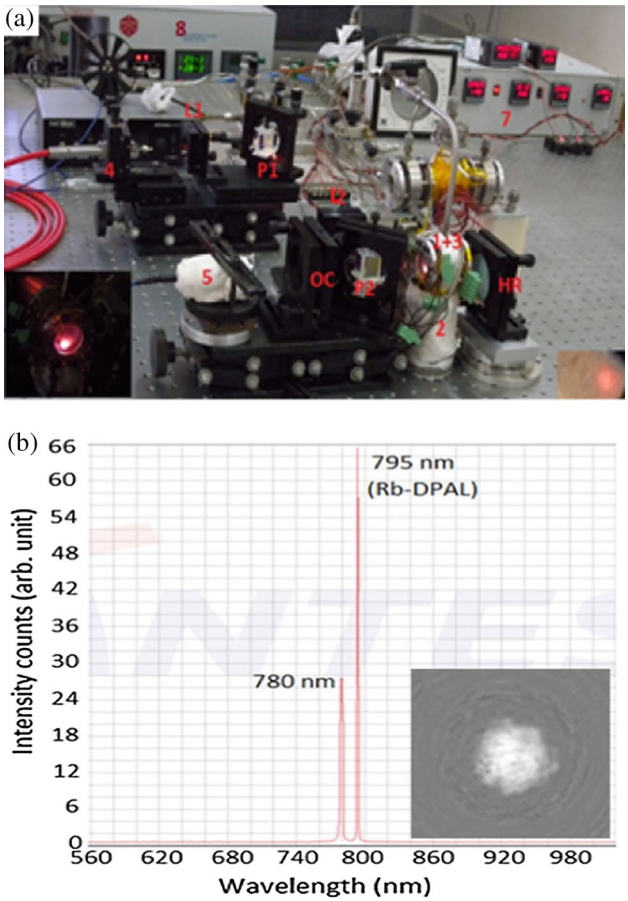

Figure 5. (**a**) Photograph of the developed Rb-DPAL system (inset: bright fluoroscence in gain medium (left) and bright spot of the Rb-DPAL output beam on the IR sensor (right)) and (**b**) typical recorded optical spectrum and image of spatial beam cross-section intensity (inset) of the developed Rb-DPAL.

conditions, the threshold values of the spectral intensity of the pump were found to be in the range of ∼0.53 to ∼2.65 kW/cm^2 nm (see §5.4).

With transition from the misaligned to the perfectly aligned condition of the resonator, both the infrared sensor as well as the CCD image showed a central bright core of the high-intensity spot of the Rb-DPAL beam with a spontaneous emission/fluorescence background. Apparently, the spectral width of the 795 nm line also reduced with significant enhancement of its intensity peak (as compared to the misaligned condition), whereas that of the 780 nm line remained almost unchanged. At the misaligned condition, the bright core of the beam cross-section image disappeared, both on the IR sensor as well as in the CCD image, and the spectral attributes of both lines (780 and 795 nm) were equivalent, as expected. The observed spatial and spectral characteristics (feedback-dependent) of the optical emission confirm the lasing action in our device

[16–18]. These observations are in sharp contrast with that of the simple fluorescence behaviours, because the former is highly directional and the latter is isotropic in nature. Furthermore, the ambiguity of partial collimation of the fluorescence in observation of the above characteristics of the Rb-DPAL is ruled out owing to the defocussing nature of thermal gas lens and the practical absence of the thermal window-lens in the present set-up (circumferential heating along with much lower power/temperature), in line with similar reported studies [19]. Quantitative assessment of the linewidths of the transitions, under lasing conditions, was not possible owing to poor resolution and accuracy of the spectrometer used in the present set-up. However, for an assessment of the laser output, the intensity peak of 795 nm line, when the optical feedback is nill (misaligned OC), was taken as the base line. The variations of the laser output intensities with the employed operating parameters are presented in the following sections.

5.2 *Effect of buffer gas pressure and composition*

The variation of the Rb-DPAL output with buffer gas pressure is shown in figure 6. The pump power, focal length of the pump-focussing lens and temperature of the rubidium reservoir were kept constant at 8 W, 10 cm and 130°C, respectively. It is observed that as the buffer gas pressure increases, the laser output increases monotonically up to a certain value of the gas pressure (dependent on composition) and then falls gradually after attaining the peak. However, the rise and fall of the laser power with buffer gas pressure is higher for higher concentrations of C_2H_6 gas. In addition, with the increase in C_2H_6 concentration, the peak shifts towards a lower pressure with increased counts of the laser output intensity. For only He, the rise of the laser output power is the slowest with maximum values at the highest pressure used (4 bar), however, without any signature of saturation. On the other hand, the peak values of the laser output are at ∼3, ∼2.5, ∼1.5, ∼1.3 and ∼1 bar pressures for the buffer gas mixtures (C_2H_6 + He) with 10, 15, 20 and 25% C_2H_6 and pure C_2H_6, respectively.

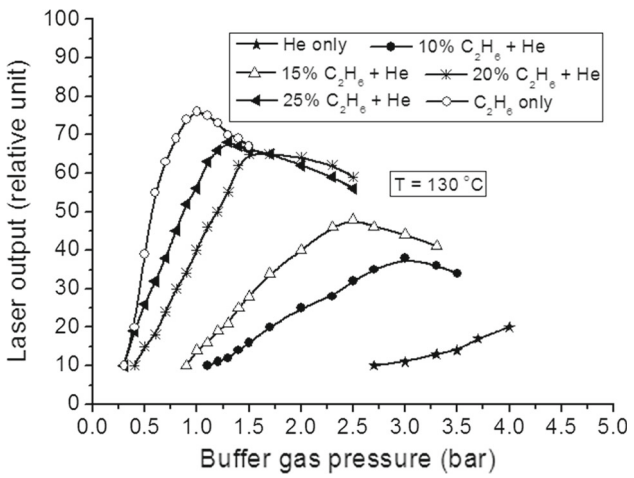

Figure 6. Variation of Rb-DPAL output intensity with pressure of different buffer gases.

The aforementioned characteristics of the Rb-DPAL can be understood as follows. In a Rb-DPAL, the buffer gas pressure plays a crucial role for pump beam absorption, spin–orbit mixing and collision quenching of the upper levels. As the pump beam passes through the Rb-DPAL gain medium, its intensity reduces from the initial value (I_o) following Beer's law $I \approx I_o e^{-\sigma n_{Rb} l}$, where l is the length of the gain medium, n_{Rb} is the ground-state density of rubidium and σ is the absorption cross-section of rubidium corresponding to its D_2 line [14,15]. Furthermore, σ is a function of the absorption linewidth ($\Delta\nu$), shift in absorption line centre (ν_o) and n_{Rb}, i.e. $\sigma \propto [(n_{Rb}\Delta\nu)/\{(\nu - \nu_o)^2 - (\Delta\nu/2)^2\}]$ [20]. The value of $\Delta\nu$ is decided by isotope shift, hyperfine splitting and broadening effects. For natural rubidium as the lasant, the D_2 transition consists of 12 hyperfine components corresponding to both of its isotopes, each of which is subjected to the broadening effects, thermal/Doppler (D), natural and pressure/Lorentzian (L), producing a Voigt profile of width [21,22]

$$\Delta\nu_i^{hf} \approx 0.5346\Delta\nu_i^{L} + \sqrt{0.2166\left(\Delta\nu_i^{L}\right)^2 + \left(\Delta\nu_i^{D}\right)^2}.$$

The convolution of the Voigt profiles of all the hyperfine lines produces the net absorption spectral width, $\Delta\nu$ (i.e. $\Delta\nu = \Sigma\Delta\nu_i^{hf}$). The isotope shift and hyperfine contributions are found to be in the range of fraction of GHz to a few GHz whereas the overall Doppler contribution is found to be ∼0.7 GHz. The pressure-broadening coefficients, corresponding to buffer gases C_2H_6 and He, are found to be ∼21.13 and ∼15.26 MHz/mbar, respectively [23,24]. For an operating regime of a Rb-DPAL, the Doppler contribution to the peak value of σ is also much smaller than that of the buffer gas (∼10^{-11} cm^2 vs. ∼10^{-9} cm^2) [23,24].

Further, the spin–orbit mixing time constant between two levels i and $j[\tau_{mix.(ij)}]$ is a function of buffer gas atom/molecule density (n_b), collision cross-section (σ_{ij}) and thermal velocity of the colliding partners ($\langle\nu_r\rangle$), i.e. $\tau_{mix.(ij)} \propto [1/(n_b\sigma_{ij}\langle\nu_r\rangle)]$ where $\langle\nu_r\rangle = \sqrt{8kT/\pi\mu}$, k is the Boltzmann constant and $\mu = m_{Rb}m_b/(m_{Rb} + m_b)$, the reduced mass of the colliding pairs [5,23]. The spin–orbit relaxation cross-section of the rubidium atom relevant for Rb-DPAL (σ_{32}:) is ∼7.7×10^{-15} cm^2 and ∼1.03×10^{-17} cm^2, respectively, for C_2H_6 and He [23,24].

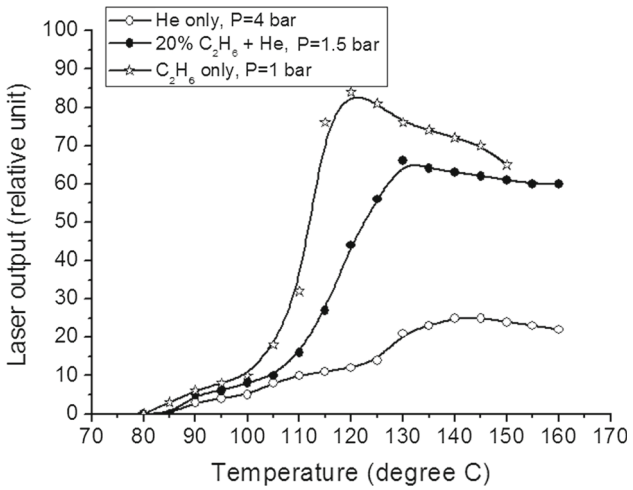

Figure 7. Variation of Rb-DPAL output intensity with laser–cell temperature for different buffer gases.

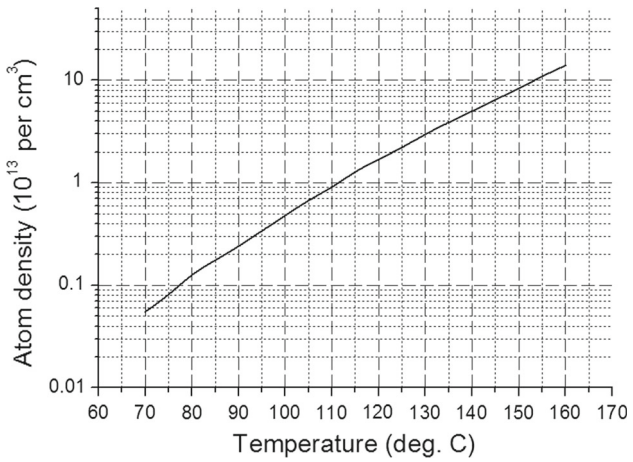

Figure 8. Variation of rubidium atom density with cell temperature.

As the buffer gas pressure increases (for all the compositions studied), the spectral width of the D_2 transition and the spin–orbit relaxation/mixing rate increases concurrently. In combination, these lead to increased pump beam absorption (pumping) and larger population inversion, giving rise to a higher laser output intensity as observed for all the cases of buffer gases (figure 6). However, the shifting of the threshold as well as the optimum pressure towards lower values, for increased C_2H_6 concentration, is attributed to higher pressure-broadening coefficients and spin–orbit relaxation/mixing cross-section of the former, which promotes faster pumping and efficient population inversion, respectively [3–5]. Similarly, the relatively faster fall of the laser output with increased C_2H_6 concentration is attributed to higher quenching (collisional) cross-section of C_2H_6 than He (σ_{31}: $\sim 6 \times 10^{-16}$ cm^2 vs. $\leq \sim 10^{-19}$ cm^2) which destroys the population inversion. The higher sensitivity of the laser output to the variation of pressure is attributed to a higher line centre (ν_o) shift coefficient of C_2H_6 than He (~ -6.6 MHz/mbar vs. $\sim +0.29$ MHz/mbar) that offsets the pump beam absorption [24]. In addition, increased quenching to the ground level ($^2P_{3/2} \rightarrow {}^2S_{1/2}$) also leads to the increased heating of the gain medium, resulting in the reduction in population inversion and increase in the pumping threshold (heating due to $^2P_{3/2} \rightarrow {}^2S_{1/2}$ quenching is more detrimental than that of $^2P_{3/2} \rightarrow {}^2P_{1/2}$ because the energy gaps are $\sim$55 times higher).

5.3 *Effect of laser-cell temperature*

The variation of the Rb-DPAL output with laser-cell temperature is shown in figure 7 for different buffer gas compositions at their optimised pressures. Only three buffer gas compositions, i.e. pure He, 20% C_2H_6 + He and pure C_2H_6, were studied with a pump power of 8 W and a focal length of 10 cm of pump focussing lens. It is observed that as the temperature of the rubidium reservoir is increased from 70 to 160°C, the laser output intensity increases slowly at the beginning followed by its rapid rise to attain a peak and then decreases. The rate of rise is the highest when the buffer gas is only C_2H_6, whereas it is the lowest when the buffer gas is only He. The peak of the output occurs at $\sim$120°C, $\sim$130°C and $\sim$140°C for the three buffer gase compositions, i.e., C_2H_6 only, 20% C_2H_6 + He and He only, respectively.

The concept of pump beam absorption can also be extended to explain these characteristics, where the absorption cross-section is also a function of ground-state rubidium density (n_{Rb}). n_{Rb} is a function of the temperature (T) of the Rb reservoir and was estimated for different T from its vapour pressure relation $n_{Rb} = N_A p/RT$ where R is the ideal gas constant ($= 6.236 \times 10^3$ cm^3 Torr/mol $\cdot$ K), N_A is the Avogadro number ($= 6.022 \times 10^{23}$ mol^{-1}) and p is the vapour pressure of Rb such that $\log_{10} p = 2.881 + 4.312 - 4040/T$ [25]. The variation of n_{Rb} for different T is shown in figure 8. As the temperature (T) increases from 70 to 160°C, the value of n_{Rb} increases from $\sim 10^{12}$ cm^{-3} to $\sim 10^{14}$ cm^{-3}. Increased n_{Rb} favours higher absorption of the pump beam and higher population inversion density leading to higher laser output. However, for fixed pump power, the decrease in laser output beyond some critical density is linked to the loss of population inversion due to the increased self-collisional quenching to the ground state. These are in line with the experimental observations of relatively lower optimal temperature of lasing in the case of only C_2H_6 than that of only He and He + C_2H_6, where the

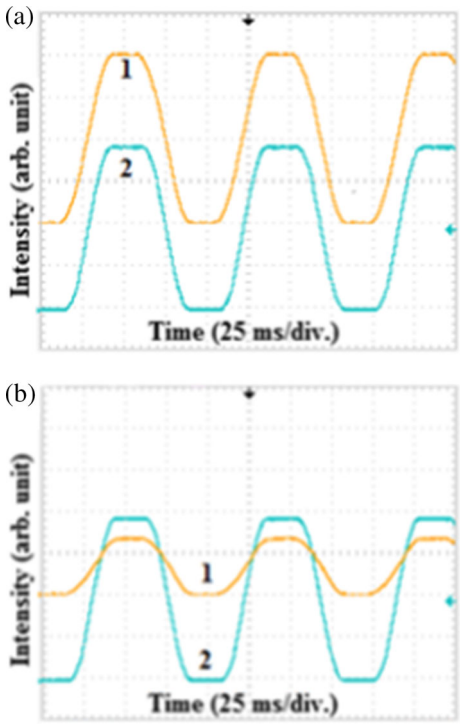

Figure 9. Chopped pump (1) and reference (2) beam through DPAL cell (**a**) at room temperature and vacuum condition and (**b**) at 130°C and He–C_2H_6 mixture in the Rb-DPAL cell.

contribution of relatively lower n_{Rb} is compensated by increased absorption linewidth. Furthermore, at a higher temperature, increased reaction of Rb with C_2H_6 (i.e. $6Rb + C_2H_6 \rightarrow 6RbH + 2C$), reduces the laser output due to the increased locking of lasant Rb atoms in the form of RbH and deposition of the products on the laser windows which reduce the transmission and increase the laser threshold [2,3].

To confirm the argument of pump beam absorption, as outlined above, the absorption efficacies were assessed experimentally, for various parametric conditions, employing a chopped pump beam as described elsewhere [26]. The chopped beam was split into two parts of almost equal power where one part was passed through the DPAL cell and the other was taken as reference. The extent of absorption was judged by comparing the intensities of these two beams using a photodiode and an oscilloscope (figures 9a and 9b). It was observed that for buffer gas compositions of C_2H_6 only, He + 20% C_2H_6 and He only, at their respective optimised conditions of temperature and pressure, the corresponding pump beam absorptions per pass in the laser cell were ~43%, ~39% and ~30%, respectively (figure 10).

5.4 *Effect of pump power and pump focal length*

The variation of the laser output intensity with pump power is shown in figure 11. Two different focal length

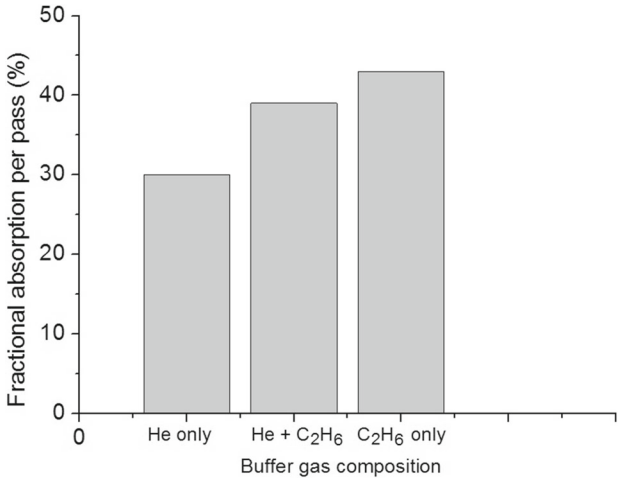

Figure 10. Variation of fractional absorption of pump beam for various buffer gas compositions.

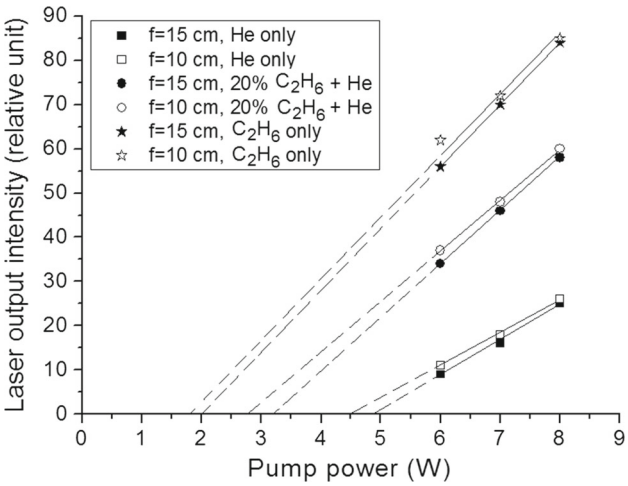

Figure 11. Variation of Rb-DPAL output power with pump power for different buffer gas compositions and pump focal lengths.

(f_2) values of the focussing lens for three different buffer gas conditions at their respective optimum pressure and temperature values, i.e. 4 bar He at 140°C, 1.5 bar He + 20% C_2H_6 at 130°C and 1 bar C_2H_6 at 120°C were used. The variation of pump power from 8 to 6 W was obtained by using suitable neutral density filters to retain the spectral characteristics of the pump beam.

It is observed that the laser output intensity is a monotonic function of pump power for all the three buffer gases and both the values of pump focal lengths. In addition, the threshold pump powers (obtained by extrapolation of lines in figure 11) and the slopes (efficiencies) are also different for different gas compositions and pump focal lengths. The threshold values of the pump power are about 4.5, 2.8 and 1.8 W for $f = 10$ cm and are about 4.9, 3.2 and 2 W for $f = 15$ cm for buffer gases with compositions of He

Table 1. Pumping conditions of the Rb-DPAL for different pump-focussing conditions.

f_2 (cm)	Pump spot diameter (μm)	Pump spectral intensity @ 8/7/6 W (kW/cm^2 nm)	DPAL gain length (mm)	DPAL gain volume (mm^3)
10	~600	~4.72/4.13/3.54	~2.71	~0.76
15	~900	~2.11/1.83/1.57	~6.11	~3.88

only, He + 20% C_2H_6 and C_2H_6 only, respectively. The slope efficiencies for a given buffer gas are equivalent for both the focal lengths (f = 10 and 15 cm). However, these values are different for different buffer gas compositions. The slopes are in the ratio of about 2:5:6 for He only, He+20% C_2H_6 and C_2H_6 only, respectively. Out of all these cases, the highest output intensity and efficiency of the Rb-DPAL is observed for 10 cm focal length at 8 W pump power (maximum used in the present case) with pure C_2H_6 as the buffer gas.

With increase in pump power, the increase in Rb-DPAL output is apparent due to increased pump spectral intensity. Increased pump intensity enhances the pumping rate (R_p), where $R_p \sim [I/(I_{sat.}\tau_{31})]$, and $I_{sat.}$ is the pump saturation intensity [24]. A change in pump focal length also changes the pumping intensity as well as the active laser gain volume, and hence change in the laser output. Higher pump intensity with higher laser active volume produces higher laser output. In the present case, for a focal length of 10 cm, the pump spot size corresponds to ~600 μm with spectral intensity values of ~3.54 kW/cm^2 nm, ~4.13 kW/cm^2 nm and ~4.72 kW/cm^2 nm whereas that for 15 cm, the pump spot size is ~900 μm with spectral intensity values of ~1.57 kW/cm^2 nm, ~1.83 kW/cm^2 nm and ~2.1 kW/cm^2 nm for pump powers of 6, 7 and 8 W, respectively (table 1). From figure 11, the threshold spectral intensity values are found to be ~2.65 kW/cm^2 nm, ~1.65 kW/cm^2 nm and ~1.06 kW/cm^2 nm for f = 10 cm and ~1.28 kW/cm^2 nm, ~0.84 kW/cm^2 nm and ~0.53 kW/cm^2 nm for f = 15 cm, corresponding to the buffer gas compositions of He only, He + 20% C_2H_6 and C_2H_6 only, respectively. These values exceed the spectral saturation intensity of ~0.43 kW/cm^2 nm [27]. For substantial laser output power and efficiency, pump spectral intensities of tens of kW/cm^2 nm are desirable [28]. However, higher intensity also increases higher state excitation and ionisation of rubidium as well as thermal lensing in the gain medium, both of which cumulatively reduce pump coupling as well as population inversion density, and, consequently, the Rb-DPAL output [29].

The increase in slope efficiency with the increase in C_2H_6 concentration is linked with the increased pump absorption and faster spin–orbit mixing, as outlined in §5.2. On the other hand, a marginal increase in laser output with the lowering of the focal length of the pumping lens (despite more than the two-fold increase in pump intensity at the same power) is linked with the lowering of the active gain volume (table 1). An increase in pump focal length increases the depth of focus [$\approx (f_2/f_1)^2(D_{core}/NA)$], and hence, the laser gain volume which is estimated to be ~2.71 and ~6.11 mm and ~0.76 and ~3.88 mm^3 for focal lengths of 10 and 15 cm, respectively [30]. For a given buffer gas composition, the benefit of the increase in gain volume by increasing the pump focal length has been offset by the reduction in pump intensity. So no substantial gain in laser output intensity has been observed in the present experiment.

The present study focussed on the investigation of relative effects of the operating parameters on the output of the Rb-DPAL designed and developed in-house. This study was carried out successfully using a photodiode (spectrophotometer) which was reliable and sensitive. The absolute laser power was not measured.

However, an upper limit of its output power was inferred to be of the order of several mW. Enhancement of the performance is expected by changing the optical resonator and optical design of the pumping configuration (for better matching of pump and mode volume and using transverse pumping), increasing the reflectivity of the OC, changing the buffer gas composition involving only He at elevated pressure and/or using better stable hydrocarbon gas such as CH_4 or mixture of both and using a pump laser of a lower linewidth. In addition, the present study was limited to polarised beam of ~8 W pump power. The use of further higher power and a lower linewidth pump diode laser will also enhance the Rb-DPAL output.

6. Conclusions

In conclusion, studies on design and parametric effects of a diode pump alkali laser, i.e. Rb-DPAL, a complex, challenging yet promising laser system, were carried out. The design and development of the laser gain cell, microheater assemblies, glove box-based alkali transfer system, gas handling system, optical set-up and

precision control instrumentation systems were carried out successfully. These subsystems were integrated. This was followed by the successful laser generation of end-pumped configuration and laser performance studies along with relevant pump beam absorption. Effects of various operating parameters such as buffer gas pressure, buffer gas composition and laser-cell temperature on Rb-DPAL output were studied experimentally. The experimental results were analysed and discussed in light of pump beam absorption, the associated laser level kinetics and effective laser gain volume.

Acknowledgements

R Biswal acknowledges the support and encouragement from Dr K S Bindra, Head, LDIAD and Mr K Ranganathan, Head, LDIAD/HPLDL.

References

[1] W F Krupke, US Patent No. 6643311 (2001)
[2] R H Page, R J Beach and W F Krupke, CMAA1, *Proceedings of the CLEO* (Baltimore, USA, 2005) p. 467
[3] R J Lane, A B Peterson and J Gloyd, CTuD6, *Proceedings of the CLEO* (Baltimore, Maryland, USA, 2007)
[4] W F Krupke, R J Beach, V K Kanz and S A Payne, *Opt. Lett.* **28**(**23**), 2336 (2003)
[5] W F Krupke, *Prog. Quant. Electron.* **36**, 4 (2012)
[6] F Gao, F Chen, J J Xie, D J Li, L M Zhang, G L Yang, J Guo and L H Guo, *Optik* **124**, 4353 (2013)
[7] B V Zhdanov and R J Knize, *Opt. Eng.* **52**(**2**), 021010 (2013)
[8] Y Wang and G An, *Proc. SPIE* **9521**, 95211 (2014)
[9] G A Pitz, D M Stalnaker, E M Guild, B Q Oliker, P J Moran, S W Townsend and D A Hostutler, *Proc. SPIE* **9729**, 972 (2016)
[10] G A Pitz and M D Anderson, *Appl. Phys. Rev.* **4**, 041101 (2017)
[11] P S Wisoff, LLNL-TR-730237 (2017), https://e-reports-ext.llnl.gov/pdf/881329.pdf
[12] W F Krupke, R J Beach, V K Kanz, S A Payne and J T Early, *Proc. SPIE* **5448**, 7 (2004)
[13] S Pradhan, R Behera and A K Das, *Pramana – J. Phys.* **78**(**4**), 584 (2012)
[14] R J Beach, W F Krupke, V K Kanz, S A Payne, M A Dubinskii and L D Merkle, *J. Opt. Soc. Am. B* **21**(**12**), 2151 (2004)
[15] N D Zameroski, G D Hager, W Rudolph and D A Hostutler, *J. Opt. Soc. Am. B* **28**(**5**), 1088 (2011)
[16] I D W Samuel, E B Namdas and G A Turnbull, *Nat. Photon.* **3**, 546 (2009)
[17] https://doi.org/10.1038/nphoton.2017.28
[18] https://www.nature.com/authors/policies/laserchecklist.pdf
[19] R Biswal, G K Mishra, G S Purbia, P K Agrawal, O Prakash, S K Dixit and J K Mittal, *Opt. Eng.* **50**(**8**), 084202 (2011)
[20] N D Zameroski, W Rudolph, G D Hager and D A Hostutler, *J. Phys. B* **42**, 245401 (2009)
[21] R Biswal, G K Mishra, P K Agrawal, S V Nakhe and S K Dixit, *Appl. Opt.* **52**(**14**), 3269 (2013)
[22] G A Pitz and G P Perram, *Proc. SPIE* **7005**, 700526 (2008)
[23] N D Zameroski, G D Hager, W Rudolph, C J Erickson and D A Hostutler, *J. Quant. Spectrum. Rad. Trans.* **112**, 59 (2011)
[24] W Y Juan, P B Liang, Z Qi and Y Jing, *Opt. Comm.* **284**, 4045 (2011)
[25] http://steck.us/alkalidata
[26] R Biswal, G K Mishra, S K Agrawal, S K Dixit and S V Nakhe, CP-1.45, *Proceedings of the NLS-25* (Bhubaneswar, 2016)
[27] R H Page, R J Beach, V K Kanz and W F Krupke, *Opt. Lett.* **31**(**3**), 353 (2006)
[28] C V Sulham, G P Perram, M P Wilkinson and D A Hostutler, *Opt. Commun.* **283**, 4328 (2010)
[29] X Zhao, Z Yang, W Hua, H Wang and X Xu, *Opt. Exp.* **25**(**8**), 9458 (2017)
[30] Th Beck, N Reng and H Weber, *Opt. Lasers Eng.* **34**, 255 (2000)